

Self-duality of One-dimensional Quasicrystals with Spin-Orbit Interaction

Deepak Kumar Sahu,¹ Aruna Prasad Acharya,¹ Debajyoti Choudhuri,² and Sanjoy Datta^{1,3,*}

¹*Department of Physics and Astronomy, National Institute of Technology, Rourkela, Odisha, India*

²*Department of Mathematics, National Institute of Technology, Rourkela, Odisha, India*

³*Center for Nanomaterials, National Institute of Technology, Rourkela, Odisha, India*

(Dated: December 31, 2021)

Non-interacting spinless electrons in one-dimensional quasicrystals, described by the Aubry-André-Harper (AAH) Hamiltonian with nearest neighbour hopping, undergoes metal to insulator transition (MIT) at a critical strength of the quasi-periodic potential. This transition is related to the self-duality of the AAH Hamiltonian. Interestingly, at the critical point, which is also known as the self-dual point, all the single particle wave functions are multifractal or non-ergodic in nature, while they are ergodic and delocalized (localized) below (above) the critical point. In this work, we have studied the one dimensional quasi-periodic AAH Hamiltonian in the presence of spin-orbit (SO) coupling of Rashba type, which introduces an additional spin conserving complex hopping and a spin-flip hopping. We have found that, although the self-dual nature of AAH Hamiltonian remains unaltered, the self-dual point gets affected significantly. Moreover, the effect of the complex and spin-flip hoppings are identical in nature. We have extended the idea of Kohn's localization tensor calculations for quasi-particles and detected the critical point very accurately. These calculations are followed by detailed multifractal analysis along with the computation of inverse participation ratio and von Neumann entropy, which clearly demonstrate that the quasi-particle eigenstates are indeed multifractal and non-ergodic at the critical point. Finally, we mapped out the phase diagram in the parameter space of quasi-periodic potential and SO coupling strength.

I. INTRODUCTION

In one dimensional (1D) lattice with random disorders, all the electronic single-particle states (SPS) of the non-interacting Anderson Hamiltonian localize exponentially even if the strength of the disorder is arbitrarily small [1, 2]. In pure Anderson Hamiltonian, metal (extended SPS) to insulator (localized SPS) transition exists only in three dimension (3D), while in two dimension (2D) there are no extended states, but for weak disorder SPS are marginally localized[2]. The extended states are also ergodic, that is, in the thermodynamic limit the real space average of the q -th moment of $|\psi(i)|^2$ converges to its ensemble average value [3]. In contrast, a quasiperiodic lattice, described by the Aubry-André-Harper (AAH) Hamiltonian [4–6] with nearest-neighbour hopping, undergoes metal to insulator (MIT) transition at a critical disorder strength, even in 1D. The fundamental, spinless AAH Hamiltonian referred above can be represented by the eigenvalue equation, $t(\psi_{n+1} + \psi_{n-1}) + W\cos(2\pi bn + \phi)\psi_n = E\psi_n$, where W is the strength of the disorder, t is the nearest neighbour hopping amplitude, and ψ_n is the amplitude of the electronic wave function at the lattice site n . When b is irrational we have the quasi-periodic lattice. The AAH Hamiltonian in reciprocal space is given by, $\frac{W}{2}(\psi_{k+1} + \psi_{k-1}) + 2t\cos(2\pi bn + \phi)\psi_k = E\psi_k$. The Fourier transformed AAH Hamiltonian becomes same as the original Hamiltonian when $W/t = 2$ and their roles are interchanged. This unique feature of AAH Hamiltonian makes it *self-dual*, as states below and above this

critical value $W_c/t = 2$ are related by Fourier transformation. All the SPS are extended for $W_c/t < 2$ while they are localized for $W_c/t > 2$. The self-dual point $W_c/t = 2$ is particularly special, as all the states show multifractal character, that is, they are extended but *non-ergodic*.

Disordered electronic systems have continued to receive wide attention, even after more than five decades of the publication of the seminal paper by Anderson [1]. A major driving force behind this is due to the importance of disorders, which are unavoidable in real materials. Also, the debate about whether MIT exists in dimension lower than three in such lattices is not settled completely. The search for MIT in lower dimensional disordered systems is not just an academic interest, but it is an extremely important problem from the point of view of device applications as well. Moreover, successful experimental simulations of these disordered Hamiltonians in optical lattice set-up [7–10] have opened the possibility of verification of the theoretical predictions. More recently, the critical behaviour of the spin-less version of the AAH Hamiltonian has been experimentally observed in polaritonic 1D wires, created with the help of cavity-polariton devices[11]. Consistent effort towards finding MIT in lower dimension have led researchers to consider Anderson Hamiltonian with SO coupling quite extensively [12–20]. However, the effect of SO coupling in quasi-periodic systems has not received much attention.

In this present work, we have explored the effect of SO coupling on MIT in quasi-periodic 1D lattice. More specifically, we have studied the AAH model with nearest neighbour hopping in the presence of Rashba type spin-orbit (RSO) coupling [21]. RSO coupled electronic systems receive wide attention because of its potential in various device applications, especially in spintronic de-

* dattas@nitrkl.ac.in

vices [22]. The main advantage of RSO coupled systems is the possibility of easier external control of the coupling strength. In order to find a comprehensive and clear answer, we have systematically used three different approaches. First, to determine the effect of RSO on the nature of MIT in 1D quasi-periodic lattice, we have used the idea of many-body localization tensor [23, 24], which is based on Kohn's idea of localization in disordered systems [25]. In the process, we have demonstrated that this many-body localization tensor, also known as Kohn's localization tensor (KLT), is a truly powerful method to study MIT for spinfull electronic systems, *where spin states mix*. After obtaining precise answer on the effect of RSO on MIT, we studied the nature of the eigenstates across the entire energy spectrum for different disorder strengths. For this we have used the inverse participation ratio (IPR) and von Neumann entropy (vNE) to get a quick overall idea about the nature of the quasi-particle eigenstates. Finally, we have carried out detailed multifractal analysis to prove that the self-duality of AAH Hamiltonian remains preserved in the presence of RSO, although the self-dual point shifts towards higher disorder strength with the increase of RSO coupling. While carrying out the multifractal analysis, we have used both periodic and open boundary conditions (OBC) to show that OBC can be used for the quasi-periodic lattices as well, effectively removing the constraint on the system sizes for numerical computation of the multifractal spectrum. To summarize our conclusions, at the end, we present the phase diagram in the parameter space spanned by the disorder strength and RSO couplings. It is important to note that in an earlier study [26], a 1D quasi-periodic AAH Hamiltonian with RSO coupling was obtained starting from a tight-binding square lattice in presence of uniform magnetic field. However, the RSO Hamiltonian used in the above mentioned reference is not same as ours. Although, it had also been concluded that the self-dual nature remains intact, but it was reported that the self-dual point remains unaffected by RSO coupling strength, while there exists two new phases, self-dual of each other, in the parameter space of disorder strength and SO coupling. These phases are characterized by coexistence of delocalized and localized states. Naturally, we have not found any evidence of these phases.

The paper is organized as follows: in Sec.III, we introduce briefly the idea of Kohn's localization tensor (KLT) for non-interacting electrons. From the KLT calculations, we can immediately identify the critical point for MIT. In Sec. IIIC, we have explored the evolution of the critical point with the RSO coupling strengths. However, these results do not provide clear idea about the nature of the SPS at the critical point. To study the nature of the SPS, we have computed the single particle IPR spectrum in Sec.IV and the von Neumann entropy (vNE) in Sec.V. To demonstrate that all the SPS are *non-ergodic* at the critical point, in Sec.VIA, we have calculated the multifractal spectrum for the three regions: below, above,

and at the critical point. Finally, in Sec.VII, we present the phase diagram with respect to the parameters that control the disorder strength and the strengths of RSO coupling.

II. AUBRY-ANDRÉ MODEL WITH RSO COUPLING

The Hamiltonian considered in this work consists of two parts,

$$H' = H + H_R, \quad (1)$$

where H is the usual AAH Hamiltonian given by,

$$H = -t \sum_{i=1,\sigma}^{L-1} (c_{i+1,\sigma}^\dagger c_{i,\sigma} + h.c.) + W \sum_{i=1,\sigma}^L \cos(2\pi b i + \phi) c_{i,\sigma}^\dagger c_{i,\sigma} \quad (2)$$

Here, t is the hopping amplitude from site i to site $i + 1$ and $L = Na$ is the length of the lattice, where N is the number of lattice sites and $a = 1$ (arbitrary unit) is the lattice spacing. $c_{i,\sigma}^\dagger$ and $c_{i,\sigma}$ are the fermionic creation and annihilation operators respectively for spin operator $\sigma = \uparrow, \downarrow$ particle at site i . W is the strength of quasi-periodic potential. ϕ is an arbitrary phase varying from $(0, 2\pi)$. The choice of the phase ϕ does not affect our conclusion, and henceforth we shall set it to zero. We have used $b = (\sqrt{5} + 1)/2$. Please note that, sometimes in the literature $b = (\sqrt{5} - 1)/2$ is also used, but our conclusions are independent of the particular choice of b .

The RSO Hamiltonian H_R is given by [27],

$$H_R = -\alpha_z \sum_{i=1,\sigma,\sigma'}^{L-1} (c_{i+1,\sigma}^\dagger (i\sigma_y)_{\sigma,\sigma'} c_{i,\sigma'} + h.c.) - \alpha_y \sum_{i=1,\sigma,\sigma'}^{L-1} (c_{i+1,\sigma}^\dagger (i\sigma_z)_{\sigma,\sigma'} c_{i,\sigma'} + h.c.), \quad (3)$$

where σ_y and σ_z are Pauli spin matrices in y - and z -direction respectively. α_y is a complex spin-conserving hopping due to the confinement in y -direction and α_z is a spin-flip hopping due to the confinement in z -directions. The hopping amplitude α_y and α_z could be different in general and they could also be site dependent. The pure RSO Hamiltonian H_R , that is studied in this work, has also been studied in the context of transport properties in quantum nanowires [28, 29]. Also, recently localization properties of attractive fermions have been studied in presence of the spin-flip component of the RSO Hamiltonian [30]. Since α_y is a spin preserving hopping process, it is expected that it will not change the self-dual nature of AAH Hamiltonian. However, it is not clear how W_c/t is going to be affected by α_y alone. On the other hand, the effect of spin-flip hopping, α_z , on the

self-duality as well as on W_c/t is not evident. Hence, we are going to focus mainly on the problem where $\alpha_z \neq 0$ and $\alpha_y = 0$. However, for completeness, we also present KLT results for $\alpha_y \neq 0$ and $\alpha_z = 0$.

III. KOHN'S LOCALIZATION TENSOR AND METAL TO INSULATOR TRANSITION

For a comprehensive analysis of the interplay of disorder and RSO coupling we have systematically used different approaches to capture the full picture. In this section, we discuss the idea of Kohn's localization tensor. It is a reliable way to characterize metallic and insulating state. Based on the idea first proposed by W. Kohn[25], Resta and Sorella [23, 24] formulated a localization tensor, alternatively called as Kohn's localization tensor (KLT). In the thermodynamic limit, it is independent of system size for insulating states, while for metallic states it diverges. For 1D AAH model with nearest-neighbour hopping and no RSO coupling, a metal to insulator transition takes place at the critical disorder strength $W_c/t = 2.0$. Recently, it has been shown [31] that the localization tensor $\lambda_{\alpha\beta}$, where α and β are the space co-ordinates, can capture this transition accurately. Furthermore, it has been shown that computation of $\lambda_{\alpha\beta}$ becomes particularly simpler for non-interacting electrons as well as for interacting electrons, if interaction is treated within mean-field approximation. However, in these two above mentioned scenarios spin states were completely decoupled. As mentioned earlier, in the presence of spin-flip hopping induced by RSO coupling, spin states mix to giving rise to quasi-particle eigenstates. Here, in this work we extended the computational approach of $\lambda_{\alpha\beta}$ for quasi-particle states and simultaneously capture the MIT, if it exists, accurately. We have presented our results for periodic and open boundary conditions. However, as we are going to see, we have found that it is not always possible to calculate $\lambda_{\alpha\beta}$ with open boundary condition.

Here, we briefly discuss the key aspects of KLT and methods to calculate it for different boundary conditions [31–33]. A more elaborate discussion on KLT and ways to compute it can be found in Ref.[32] and in Ref.[34]. For periodic boundary condition (PBC), the localization tensor, $\lambda_{\alpha\beta}$ (here $\alpha = x, \beta = x$) can be expressed as,

$$\lambda_{xx}^2 = -\frac{L^2}{4\pi^2 N} \ln \frac{|z_N^x| |z_N^x|}{|z_N^{xx}|}, \quad (4)$$

where the quantity z_N^x is given by,

$$z_N^x = \langle \Psi | e^{i\frac{2\pi}{L} \hat{\mathbf{R}}_x} | \Psi \rangle, \quad (5)$$

whereas, $z_N^{\alpha\beta}$ can be obtained by replacing \hat{R}_α with $\hat{R}_\alpha - \hat{R}_\beta$. Hence, in our case $|z_N^{xx}| = 1$. In the above equation, $|\Psi\rangle$ is the many-body ground state wave function, $\hat{\mathbf{R}} = \sum_{i=1}^N \hat{r}_i$ is the many-body position operator with $\hat{\mathbf{R}}_x$

being the x component. N is the number of lattice sites, while $L = N a$, with $a = 1$ (in arbitrary unit) being the lattice constant, is the size of the system. For a half-filled system ($L = N$) in 1D, the localization tensor reduces to

$$\lambda_{xx}^2 = \lambda^2 = -\frac{L}{2\pi^2} \ln \{|z_N|\}. \quad (6)$$

In absence of electron-electron interaction, $z_N^{(x)}$ can be simplified further [32, 33] and represented as $z_N^{(x)} = \det^2[S_{jj'}^x]$, where $S_{jj'}^x$ is a matrix whose elements are given by,

$$S_{j,j'}^x = \int dr \psi_j^*(r) e^{i\frac{2\pi}{L} \hat{r}_x} \psi_{j'}(r). \quad (7)$$

In the above equation $\psi_j(r)$ represents the amplitude of single-particle wave function at position r for a spin-up or spin-down electron arranged in ascending order in energies. The indices j and j' indicate the energy level. Since, in absence of RSO spin-up and spin-down electrons are completely decoupled, it is sufficient to consider only one type of spin and $j, j' = 1, 2, \dots, N/2$ to compute λ_{xx}^2 at half-filling. But, in presence of RSO, more specifically because of the spin-flip hopping process, in Eq. 7 $\phi_j(r)$ now represents the amplitude of a single quasi-particle wave function at position r corresponding to the j^{th} eigenenergy. Hence, in our case $j, j' = 1, 2, \dots, N$.

In case of open boundary conditions (OBC), squared localization length (λ^2), in units of the nearest-neighbour distance, can be expressed as follows [34, 35]:

$$\lambda^2 = \frac{1}{\nu N} \sum_{i,i'=1}^N \rho_{ii'}^2(\nu) (i-i')^2, \quad (8)$$

where $i, i' = 1, \dots, N$ represent the lattice site, ν is the filling factor and $\rho_{ii'}(\nu)$ is the one-body density matrix, defined as

$$\rho_{ii'} = \sum_{j=1}^N \phi_j(i) \phi_j^*(i'), \quad (9)$$

where $\phi_j(i)$ is the amplitude of single quasi-particle wave function at lattice site i corresponding to j^{th} eigenvalue. Since we are interested to compute λ^2 at half-filling, we set $\nu = 1$ in Eq. 8.

A. Localization tensor without RSO

Before presenting the localization tensor results for our Hamiltonian, in this section we first benchmark our λ^2 calculations for pure AA model without the RSO coupling at half-filling. We also highlight the behaviour of λ^2 with system sizes at the critical point. In Fig.1(a) and Fig.2(b), we have shown these calculation for open and periodic boundary conditions respectively. In case of PBC, system sizes are restricted to lattice sizes given by

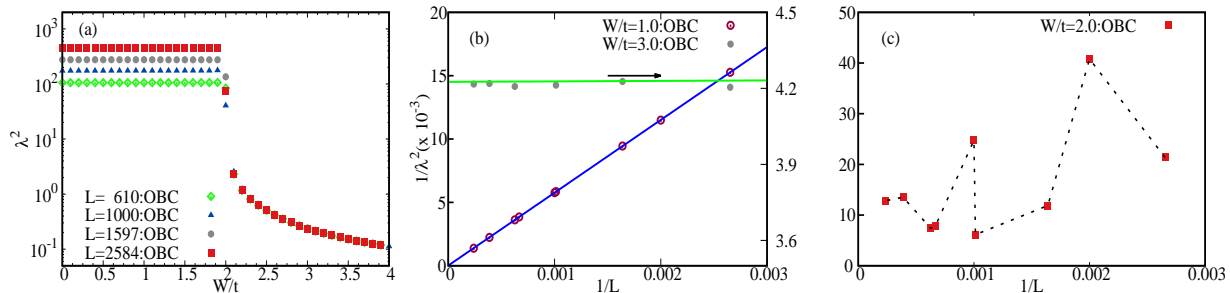


Figure 1. (a) Squared localization length λ^2 for half-filled 1D pure AA model with respect to disorder strength W/t for some selected lattices. (b) Scaling of inverse localization length $1/\lambda^2$ with inverse chain length ($1/L$). For finite size scaling we have used $1/\lambda^2 = a_0 + b_0/L$. (c) Plot of $1/\lambda^2$ with $1/L$ at the critical point. It is evident that at the critical point, $1/\lambda^2$ does not follow the scaling pattern of either metallic or insulating states. All the results for open boundary condition.

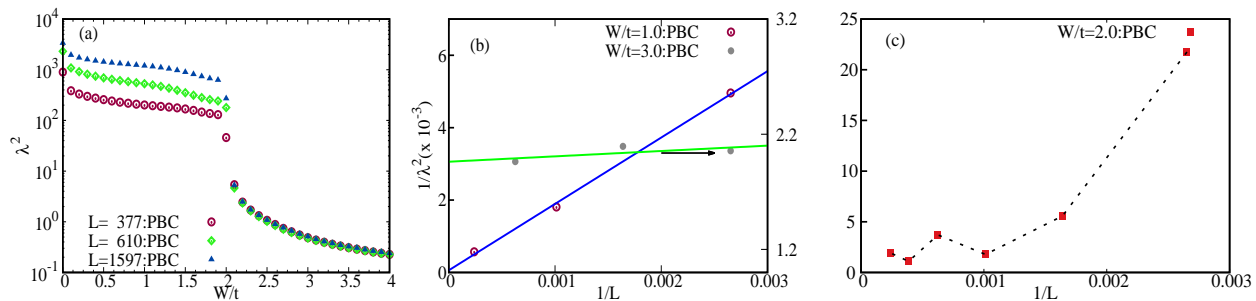


Figure 2. Localization tensor λ^2 for half-filled 1D pure AAH model with PBC. (a) λ^2 vs. W/t for a few selected chain lengths. (b) Finite size scaling of $1/\lambda^2$ vs. $(1/L)$. (c) Once again, similar to the OBC case, $1/\lambda^2$ lacks simple scaling behaviour with $1/L$ at the critical point.

the Fibonacci sequence, while for OBC there is no such restriction. One of the main objectives to compare results of different boundary conditions is to show that the localization tensor is a robust indicator to differentiate metallic and insulating state irrespective of the boundary conditions. This observation is going to be useful, as we are going to show in Sec.VI, while computing the multifractal spectrum for quasi-periodic lattices, as we do not need to restrict ourselves to very specific system sizes dictated by the Fibonacci sequence in order to extrapolate the results to thermodynamic limit.

In Fig.1(a)(OBC) and Fig.2(a)(PBC), we have shown the variation of squared localization length λ^2 with increasing disorder strength (W/t) for different 1D lattices at half-filling. As expected, the transition from delocalized to localized phase occurs at $W_c/t \simeq 2$ for both the boundary conditions. λ^2 values are finite and independent of system sizes above $W/t > 2$ whereas for $W/t < 2$, it increases with the increase of system size. These observations are similar to Ref. [31]. In Sec.III it has been mentioned that in case of metallic phase λ^2 diverges in the thermodynamic limit, while it is independent of system sizes in the insulating phase. From the plot of $1/\lambda^2$ vs. $1/L$ of Fig. 1(b) and Fig.2(b), it is clear that, irrespec-

tive of the boundary condition, λ^2 diverges for $L \rightarrow \infty$ in the metallic phase, while it is nearly constant and converges to a finite value in the insulating phase. For pure AA Hamiltonian, we have found that $1/\lambda^2$ scales linearly with the inverse of the system size. For finite size scaling, in this case, we have used $1/\lambda^2 = a_0 + b_0/L$, where a_0 and b_0 are two adjustable parameters.

At the critical point $W_c/t = 2$, scaling behaviour of λ^2 with increasing system size is expected to be erratic as all the single particle eigenstates are multifractal in case of pure AA model. However, it can be a useful and quick indicator to detect the existence of multifractal eigenstates within a spectrum. Since there is no characteristic length-scale for multifractal states, we can expect an anomalous behaviour of $1/\lambda^2$ with respect to $1/L$ compared to pure metallic and insulating phases. In Fig. 1(c) and in Fig. 2(c) we have plotted $1/\lambda^2$ versus $1/L$ for $W_c/t = 2$. In case of OBC, it is clear that λ^2 neither converges to a finite value nor does it go to zero in the thermodynamic limit. With PBC as well, λ^2 oscillates with increasing L without any indication of convergence. In this work, however, we have used a well established and computationally less costly approach for the multifractal analysis of the eigenstates.

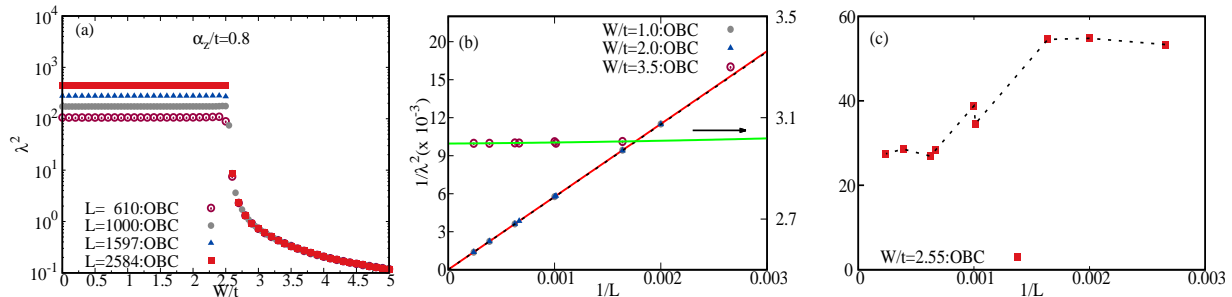


Figure 3. Localization tensor λ^2 for half-filled 1D AAH model with RSO coupling. (a) λ^2 vs. W/t for selected lattices with OBC. (b) Scaling of inverse localization length $1/\lambda^2$ vs. $1/L$. Here $1/\lambda^2$ scales linearly with $1/L$ similar to Fig. 1(b). (c) Plot of $1/\lambda^2$ vs. $1/L$ at the critical point $W_c/t = 2.55$. Lack of proper scaling of $1/\lambda^2$ indicates that our estimation of critical point is quite correct.

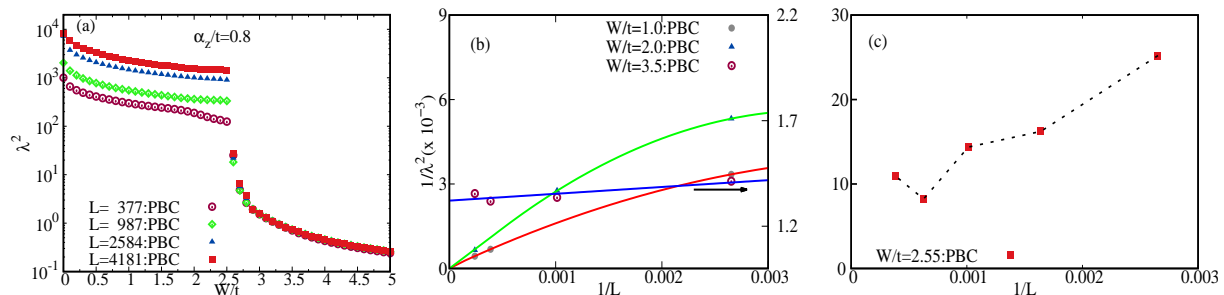


Figure 4. Localization tensor λ^2 for half-filled 1D AAH model with RSO coupling. (a) λ^2 vs. W/t for selected lattices with PBC. (b) Finite size scaling of $1/\lambda^2$ with inverse chain length $1/L$ below and above the critical point. We have used $1/\lambda^2 = a_0 + b_0/L + c_0/L^2$ for the purpose of scaling in the metallic phase. (c) With PBC as well we find anomalous behaviour of $1/\lambda^2$ with increasing system size at $W/t = 2.55$.

B. Localization tensor in presence RSO

We now present our localization tensor results for one-dimensional AA model in the presence of RSO coupling. Since the effect of the spin-flip hopping process, induced by RSO, on the self-duality is much harder to anticipate, we primarily focus on the $\alpha_y = 0$ case. We have chosen $\alpha_z/t = 0.8$. There is nothing special about this value, as all our conclusions are independent of it, except the location of self-dual point. In Fig.3(a)(OBC) and 4(a)(PBC) the variation of squared localization length, λ^2 , with increasing value of disorder strength W/t have been shown. It is evident that inclusion of RSO coupling enhances the critical point towards larger disorder strength, in this case $W_c/t \simeq 2.5$, as compared to pure AA model ($W_c/t \simeq 2$). Furthermore, this conclusion is independent of the applied boundary conditions on the system.

To confirm our observation in the thermodynamic limit we have done finite size scaling of $1/\lambda^2$ with different system sizes below and above the critical point. These results are presented in Fig. 3(b) and in Fig. 4(b). In the case of OBC, it is evident that $1/\lambda^2$ converges to

zero as $L \rightarrow \infty$ for $W/t < 2.5$, that is, for delocalized phase, while it is independent of system size for $W/t > 2.5$, indicating an insulating phase. In case of PBC also, these fundamental conclusions remain same. Interestingly, however, with PBC the dependence of $1/\lambda^2$ on $1/L$ deviates significantly in the presence of RSO in the metallic phase. For finite size scaling, specially for the metallic phase, we have used $1/\lambda^2 = a_0 + b_0/L + c_0/L^2$, where a_0, b_0 and c_0 are adjustable parameters.

It is easy to pinpoint the critical disorder strength from the λ^2 vs W/t data almost exactly. We are going to see that this information can reliably be extracted from the multifractal analysis (Sec. VIA) as well. From the localization tensor result we estimate $W_c/t \simeq 2.55$ for $\alpha_z/t = 0.8$. To cross-check this estimation, we have plotted $1/\lambda^2$ versus $1/L$ separately at $W_c/t \simeq 2.55$ in Fig. 3(c) and in Fig. 4(c). It is quite clear that $1/\lambda^2$ does not follow any discernible pattern with $1/L$. This, as we have pointed out in Sec. III A, is the hallmark of critical/multifractal eigenstates.

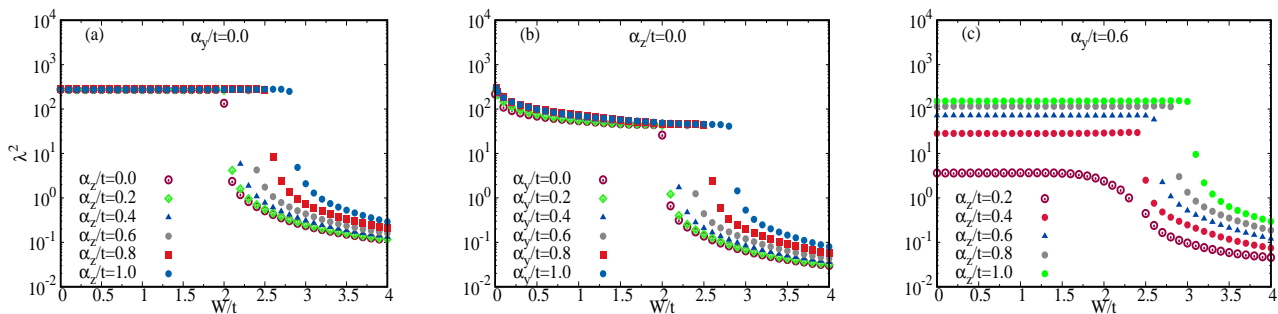


Figure 5. (a) Evolution of the self-dual point in AAH with only spin-flip hopping induced by RSO coupling. The results are for a lattice $L = 1597$ with OBC. (b) The self dual point moves towards higher strength of the quasi-periodic potential when pure AAH Hamiltonian is considered with only the complex hopping induced by the RSO coupling. (c) Evolution of the self-dual point when the AAH Hamiltonian is considered with the full RSO Hamiltonian. Here we have only shown the change with the spin-flip hopping while the complex hopping has been fixed at a value 0.6.

C. Evolution of the critical point with RSO interaction

In this section, we study the evolution of the critical point for three different cases, (i) $\alpha_y = 0$, (ii) $\alpha_z = 0$ and (iii) $\alpha_z \neq 0, \alpha_y = \text{fixed}$. For case (i) and (iii) a lattice with $N = 1597$ and OBC have been used, while for case (ii) we have used PBC and $N = 987$. It is important to note that λ^2 could not be computed with OBC for case (ii). In Fig. 5(a), we have considered only the spin-flip hopping α_z in the RSO Hamiltonian. It is clear, even from the results for a single finite lattice, that the critical point moves to higher strength of the quasi-periodic potential. Interestingly, when only the complex hopping of the RSO Hamiltonian is considered along with pure AA Hamiltonian, similar variation of the critical point is observed in Fig. 5(b). Fig 5(c), represents the general nature of the evolution of the critical point when the full RSO Hamiltonian is considered along with pure AA Hamiltonian. In these results, variation of the critical point with spin-hopping has been studied for a fixed strength of the spin conserving complex hopping having the amplitude $\alpha_y/t = 0.6$. For $\alpha_z = 0.2$, λ^2 appears to indicate a cross-over rather than a clear transition. However, this is an artifact of the finite system being used for these calculations. We have checked that as the system size is increased, a clear transition from delocalized to localized transition emerges.

IV. INVERSE PARTICIPATION RATIO

Existence of MIT in presence of RSO is evident from the results of the localization tensor calculations. Although at the critical point, anomalous behaviour of the localization tensor with the inverse of the system size do indicate the absence of a characteristic length scale, the true nature of the quasi-particle eigenstates across the entire energy spectrum is not clear. For example, if an en-

ergy spectrum contains predominantly delocalized states then the localization tensor can suppress the contribution of localized states while calculating it upto certain filling fraction. To distinguish localized and delocalized states, Inverse Participation Ratio (IPR) is regularly used as a first indicator. IPR can also provide some hint, although only qualitatively, of multifractal eigenstates, if it exists. Generally, IPR is used to quickly identify the existence of mobility-edge. Typically the mobility edge is defined as the energy which separates localized and delocalized eigenstates in the energy spectrum. If a mobility edge exists, IPR jumps from system size independent (insulating/localized states) higher value to a lower value (ergodic metallic/extended states) that scales inversely with the system size. In our case, we have observed that away from the critical point, the states are either delocalized ($W < W_c$) or localized ($W > W_c$). The other important question that remains to be answered is, what are the nature of the eigenstates at the critical point? In AA model without RSO, all the eigenstates are extended but non-ergodic at the critical point. IPR data qualitatively indicates that RSO does not alter this behaviour. At this point we would like to mention that, studying the single particle energy spectra E_n and the distribution of the level-spacing $\delta_n = E_{n+1} - E_n$ can also reveal a great deal about the nature of the eigenstates [36–38]; for example, in AAH model the energy level-spacing follows Poissonian distribution, while at the critical point this distribution follows an inverse power law. Typically, the energy spectrum of AAH Hamiltonian consists of subbands and many gaps between these subbands. Recently, it has been reported that there are some special states inside these subband gaps [39], which are localized even in the metallic phase of pure AAH Hamiltonian. We have checked that these states are mostly concentrated at the lattice edges. Appearance of these states depends on many factors; for example, they can appear for system with OBC, with PBC, but the system size is not same as certain (not all) Fibonacci number. These states do

not influence the critical behaviour in any way, as can be seen from the results of the previous section.

Formally, for ν -th quasiparticle eigenstate the usual definition of IPR [40] can be generalized as follows;

$$P_\nu(q) = \sum_{\sigma} \sum_{i=1}^N |\psi_{\nu,\sigma}(i)|^{2q}, \quad q = 2. \quad (10)$$

Here ν th single quasiparticle eigenstate is given by $|\Psi_\nu\rangle = \sum_{\sigma} \sum_{i=1}^N \psi_{\nu,\sigma}(i) |1, \sigma\rangle_i$, where $|1, \sigma\rangle_i = |0, 0, \dots, \sigma_i, \dots, 0, 0\rangle$ represents the localized basis state having one particle with spin σ at site i . Since, this is a non-interacting problem, usual scaling properties with respect to system size is also expected to hold for the quasiparticle states, i.e. for a perfectly extended metallic state $P_\nu(q) = 1/N$, and for a completely localized state $P_\nu(q) = 1$. For a localized state, the IPR value is supposed to be system size independent. These distinct scaling properties of IPR enables it to identify delocalized and localized states quickly. We have numerically verified that the spin-up and spin-down contributions are identical towards the IPR of the quasiparticle they constitute.

In Fig. 6 we have plotted the IPR spectrum for (a) $W/t = 2.5$, (b) $W/t = 2.55$, and (c) $W/t = 2.6$. These results are for $\alpha_z/t = 0.8$, $\alpha_y/t = 0$. It is evident that for $W/t < 2.55$, all the eigenstates are delocalized as the IPR value in this region depends inversely on the system size across the entire energy spectrum, while all the states are localized for $W/t > 2.55$. On the other hand, at the critical point the IPR spectrum behaves differently, it is neither independent of system size nor does it scale inversely with L like the extended states. This behaviour is similar to the IPR spectrum of AA model without RSO at the critical point, i.e. these are multifractal or in other words extended yet *non-ergodic*. Furthermore, the correlation between the energy level-spacing spectra and the scaling behaviour of IPR with L for all three different types of electronic states are similar to the AA model without RSO [39]. In the delocalized phase, IPR typically behaves inversely with L across the whole energy-spectrum except at the special positions where the level-spacing jumps abruptly. At the critical point, both of them show anomalous behaviour with the system size, while in the localized phase IPR spectrum behaves opposite compared to the delocalized phase at these special point of level-spacing spectra apart from being system size independent. All of these results are presented for PBC. OBC does not change the fundamental conclusions.

V. VON NEUMANN ENTROPY

From the results of the previous sections, it is evident that at half-filling there is a transition from metallic phase to an insulating phase at a critical disorder strength $W_c/t > 2.0$, which increases as the strength of RSO is increased. Furthermore, these results also hint

that at the critical point the states are multifractal, a preliminary observation that we are going to establish firmly in Sec. VI. In this section, we present the results of von-Neumann entropy (vNE), an alternative indicator of single particle properties, which can also be used to qualitatively identify the nature of the eigenstates.

In case of non-interacting spin-1/2 fermions, and in presence of RSO coupling, individual eigenstates are occupied by quasiparticles. The quasiparticle eigenstate having energy E_ν can be written as,

$$|\Psi_\nu\rangle = \sum_{i=1}^N [\psi_{i,\uparrow}^\nu |1, \uparrow\rangle_i + \psi_{i,\downarrow}^\nu |1, \downarrow\rangle_i], \quad (11)$$

where $|1, \uparrow\rangle_i = |1\rangle_i \otimes |\uparrow\rangle$ and $|1, \downarrow\rangle_i = |1\rangle_i \otimes |\downarrow\rangle$. $|1, \uparrow\rangle_i = c_{i,\uparrow}^\dagger |0\rangle$ and $|1, \downarrow\rangle_i = c_{i,\downarrow}^\dagger |0\rangle$. Here $|0\rangle$ represents the vacuum state for the lattice in real space basis. $c_{i,\uparrow}^\dagger$, $c_{i,\downarrow}^\dagger$ are the creation operators for spin up and spin down particles respectively at the lattice site i . The average number of spin up and down particles at site i are given by $|\psi_{i,\uparrow}^\nu|^2 = \langle \Psi_\nu | c_{i,\uparrow}^\dagger c_{i,\uparrow} | \Psi_\nu \rangle$ and $|\psi_{i,\downarrow}^\nu|^2 = \langle \Psi_\nu | c_{i,\downarrow}^\dagger c_{i,\downarrow} | \Psi_\nu \rangle$ respectively. Then, the local density matrix ρ_j^ν can be obtained from the total density matrix ρ^ν by tracing over all the lattice sites except site j and can then be written as,

$$\rho_j^\nu = |\psi_{j,\uparrow}^\nu|^2 |1, \uparrow\rangle_j \langle 1, \uparrow|_j + (1 - |\psi_{j,\uparrow}^\nu|^2) |0, \uparrow\rangle_j \langle 0, \uparrow|_j + |\psi_{j,\downarrow}^\nu|^2 |1, \downarrow\rangle_j \langle 1, \downarrow|_j + (1 - |\psi_{j,\downarrow}^\nu|^2) |0, \downarrow\rangle_j \langle 0, \downarrow|_j \quad (12)$$

It is important to note that $|0, \uparrow\rangle_j$ and $|0, \downarrow\rangle_j$ represent local vacuum states for j -th site. A similar interpretation applies to the states $|1, \uparrow\rangle_j$ and $|1, \downarrow\rangle_j$. The von Neumann entropy for spin-1/2 quasiparticles follows easily from Eq. 12 as,

$$S_{j,\nu}^{mis} = - (|\psi_{j,\uparrow}^\nu|^2 \log_2 |\psi_{j,\uparrow}^\nu|^2 + (1 - |\psi_{j,\uparrow}^\nu|^2) \ln(1 - |\psi_{j,\uparrow}^\nu|^2)) + - (|\psi_{j,\downarrow}^\nu|^2 \ln |\psi_{j,\downarrow}^\nu|^2 + (1 - |\psi_{j,\downarrow}^\nu|^2) \ln(1 - |\psi_{j,\downarrow}^\nu|^2)) \quad (13)$$

Finally summing over all the lattice sites, the von-Neumann entropy for a quasiparticle eigenstate is defined as,

$$S_\nu^{mis} = \sum_{j=1}^N S_{j,\nu}^{mis}. \quad (14)$$

Similar to the spinless AA model, for a purely extended quasi-particle state $S_\nu^{mis} \approx (\log_2 N + 1)$ and for completely localized state it is ≈ 0 .

In Fig. 7(a)-(c) results of our von Neumann entropy calculations are presented for $\alpha_z/t = 0.8$ and $\alpha_y/t = 0.0$. To show the dramatic change in vNE as we move slightly away from the critical point ($W_c/t \simeq 2.55$), in Fig. 7(a) and in Fig. 7(c) we have plotted our results for $W/t = 2.5$ and $W/t = 2.6$ respectively. It is clear that for $W/t = 2.5$ the von Neumann entropy increases with system size and roughly scales as expected, while it is independent of the

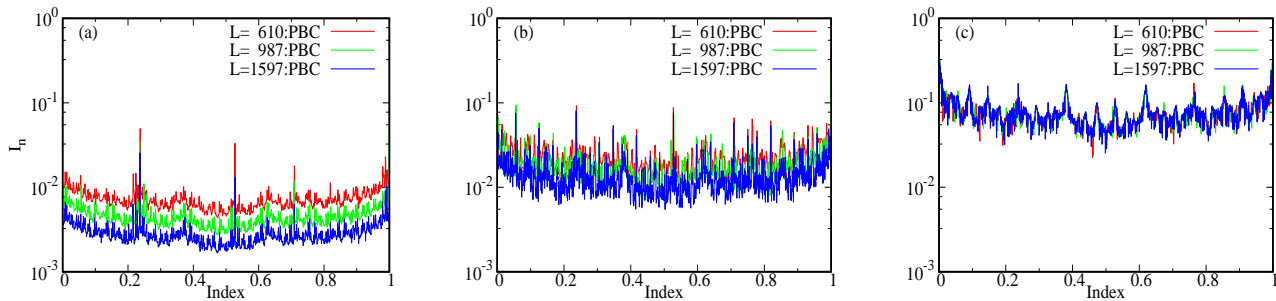


Figure 6. Evolution of IPR I_n with increasing disorder strength for a fixed RSO coupling $\alpha_z/t = 0.8$ and $\alpha_y = 0$. (a) $W/t = 2.5$, (b) $W/t = 2.55$, and (c) $W/t = 2.6$. Here index represents the ratio of serial number of eigenstate to total number of eigenstates ($i/(2L)$), where $i = 1, 2, \dots, 2L$.

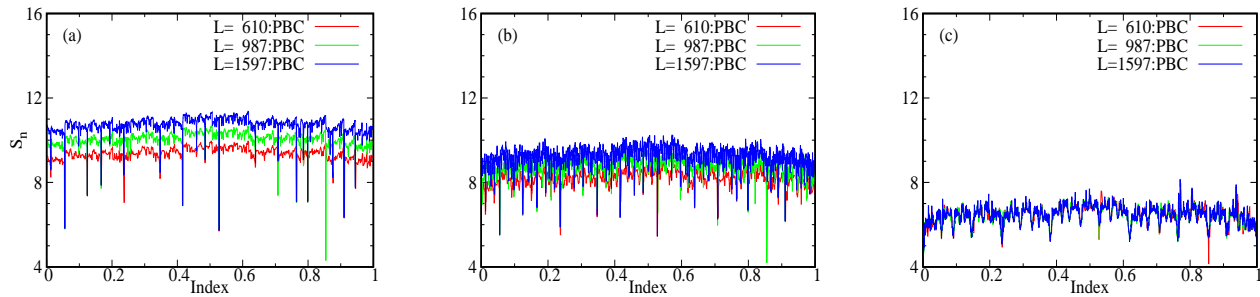


Figure 7. Evolution of von Neumann Entropy S_n with increasing disorder strength for a fixed RSO coupling $\alpha_z/t = 0.8$ and $\alpha_y = 0$. (a) $W/t = 2.5$, (b) $W/t = 2.55$, and (c) $W/t = 2.6$.

system sizes and the value is close to zero for $W/t = 2.6$. It is clear from the results of Fig. 7(b), at the critical point these results do not completely follow the expected pattern of purely extended or localized states. These results along with the localization tensor calculations and IPR data qualitatively capture the nature of the eigenstates at the critical point. However, it is necessary to have a more rigorous analysis to quantify the degree of multifractality of the eigenstates at the critical point. To address this, in the next section, we present a detail and careful analysis of the multifractal spectrum around the critical point.

VI. MULTIFRACTAL SPECTRUM AND THE QUASI-PARTICLE EIGENSTATES

“Absence of length scale” at the critical point of a phase transition has led to the understanding that localization-delocalization (LD) transition can also be viewed as a class of a much broader set of critical phenomena. Typically, the critical phenomena are characterized by critical exponents. In case of LD transition, multifractal analysis of the eigenstates plays a similar role like the critical exponents. Following the arguments of multifractal analysis [41] in our case, we start by identifying the q -th mo-

ment of the probability of finding a quasiparticle within a linear box of length L ($L = Na$, $a = 1$ in arb. unit) is $P(q) = \sum_{i=1}^N |\psi_n(i)|^{2q} \propto N^{-\tau(q)}$, where ψ_n is the quasiparticle wave function corresponding to n -th eigenvalue and $i = 1, 2, \dots, N$. The exponent $\tau(q)$ is alternatively expressed in terms of $D(q)$ as

$$\tau(q) = D(q)(q - 1), \quad (15)$$

where $D(q)$ is called the generalized dimension. In case of ergodic extended (EE) eigenstates [41] $\tau(q) = q - 1$. This conclusion follows from the argument that the real space average $P(q)/N$ converges to the ensemble average $\langle P_q \rangle / N = \langle |\psi_n(i)|^{2q} \rangle$ in the limit $N \rightarrow \infty$. Effectively it means that for EE states, $D(q) = 1$, whereas for a completely localized eigenstate $D(q) = 0$. For multifractal states, $\tau(q)$ deviates from these two limiting cases leading to q dependence of the generalized dimension $D(q)$. These states are extended yet *non-ergodic*. Out of the possible set of generalized dimensions, $D(2)$ is frequently used to characterize different states. In practice, however, instead of computing $\tau(q)$ directly, an equivalent quantity $f(\alpha)$ is evaluated. It characterizes the multifractal property of the eigenstates. $f(\alpha)$ and $\tau(q)$ are connected by the Legendre transformation,

$$f(\alpha(q)) = q\alpha(q) - \tau(q), \quad (16)$$

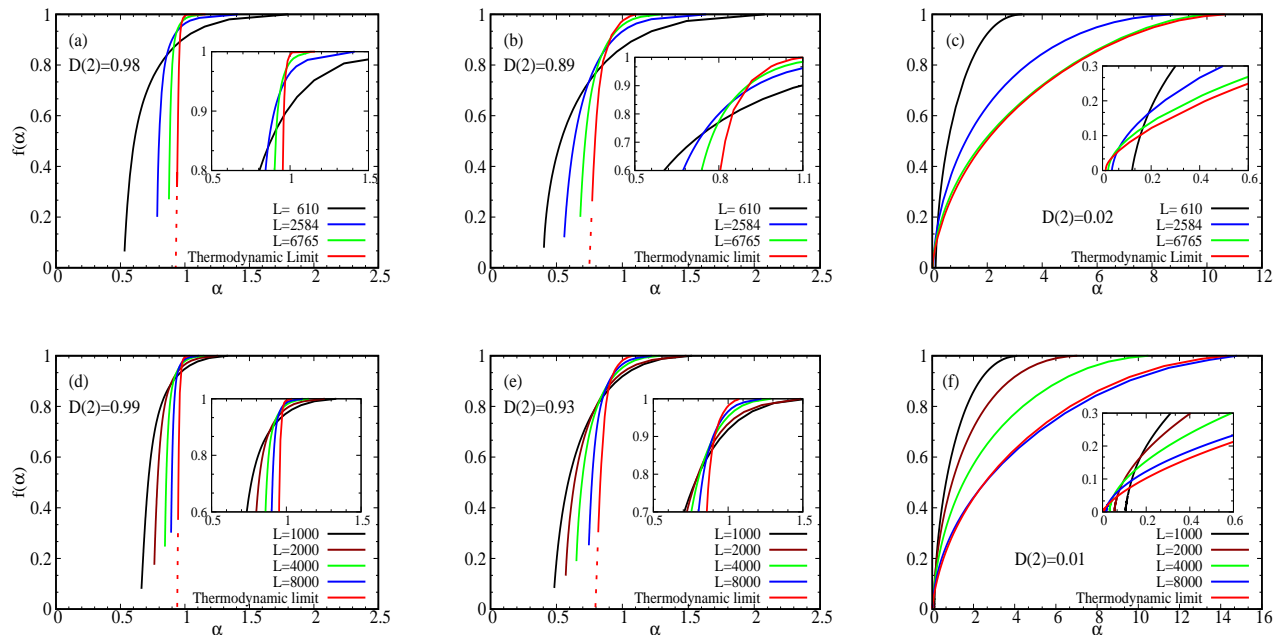


Figure 8. Multifractal spectrum of AAH Hamiltonian with RSO coupling for PBC (top row) and OBC (bottom row). Here $\alpha_y/t = 0$ and $\alpha_z/t = 0.8$. From left to right: (a, d) $W/t = 2.5$, (b, e) $W/t = 2.55$ and (c, f) $W/t = 2.6$. $D(2)$ is the generalized dimension $D(q)$ for $q = 2$. For extended ergodic states $D(2) = 1$ and $D(2) = 0$ for insulating states, while for multifractal/non-ergodic extended states $0 < D(2) < 1$.

where $\alpha(q) = d\tau(q)/dq$. In general, $f(\alpha)$ is a smooth non-monotonic positive valued function having negative curvature and a global maxima but no local minima or maxima. In fact, $f_{max} = f(\alpha(q = 0)) = d$, where d is the Euclidean dimension of the system [42]. From the analysis of the function $f(\alpha)$, one can easily identify the nature of the eigenstates. For EE states, in the thermodynamic limit $f(\alpha = 1) = 1$, while $f(\alpha \neq 1) = -\infty$. For non-ergodic (NE) eigenstates $f(\alpha(q)) \rightarrow 0$ for $0 < \alpha_{min} < \alpha(q) < \alpha_{max}$, while $f_{\alpha(q=0)} = f_{max}$ appears for $\alpha(q = 0) > 1$. In contrast to EE and NE states, for insulating states $f(\alpha(q)) \rightarrow 0$ as $\alpha(q) \rightarrow 0$, while $\alpha(q = 0)$, i.e., the position of the maxima of $f(\alpha)$ spectrum shifts towards larger value than 1 as the disorder strength is increased. It is quite evident that to identify the nature of the quasi-particle eigenstates it is sufficient to have an estimation of α_{min} ($f(\alpha_{min}) \rightarrow 0$) and $\alpha(q = 0)$ ($f_{max} = f(\alpha(q = 0)) = d$). This allows us to use a well-established method [42, 43] to compute the multifractal spectrum for our Hamiltonian. This spectrum is computed and compared for PBC and OBC. Both of these boundary conditions lead to identical conclusions.

A. Calculation of Multifractal Spectrum

Before discussing the results, we briefly summarize the key steps of to compute the multifractal spectrum. Initially the lattice is divided into small boxes of linear

size $l < L$. The first step is to find the normalized box-probability,

$$\mathcal{P}_k(l, q) = \frac{\mathcal{P}_k^q(l)}{\sum_{j=1}^{N_b} \mathcal{P}_j^q(l)}, \quad (17)$$

where $1 \leq k \leq N_b = L/l$ represents the k -th box and $\mathcal{P}_k(l, q) = \sum_{i \in l_k} |\psi_n(i)|^{2q}$, $l_k = l \forall k$, is the probability of the n -th eigenstate. Then $\alpha(q, L)$ and $f(\alpha(q, L))$ are obtained from the following relations;

$$\alpha(q, L) = \lim_{\delta \rightarrow 0} \frac{\sum_{k=1}^{N_b} \mathcal{P}_k(l, q) \ln(\mathcal{P}_k(l, 1))}{\ln \delta} \quad (18)$$

$$f(\alpha(q, L)) = \lim_{\delta \rightarrow 0} \frac{\sum_{k=1}^{N_b} \mathcal{P}_k(l, q) \ln(\mathcal{P}_k(l, q))}{\ln \delta}, \quad (19)$$

where $\delta = l/L$. It is important to note that this method of computing the multifractal spectrum is valid for $a \ll l < L$. For different system sizes L , we have chosen l in a way that the above condition is satisfied and $0.1 \leq \delta \leq 0.5$. $\alpha(q, L)$ and $f(\alpha(q, L))$ have been computed for system size upto $L = 8 \times 10^3$ and averaged over the entire energy window till half filling. Finally, the thermodynamic limit value of $\alpha(q) = \lim_{L \rightarrow \infty} \alpha(q, L)$ and $f(\alpha(q)) = \lim_{L \rightarrow \infty} f(\alpha(q, L))$ have been estimated using finite size scaling. For finite size scaling, we propose the following set of functions for $\alpha_q(L)$ and $f(\alpha_q(L))$,

$$\begin{aligned} \alpha_q(L) &= \alpha_q + a_q L^{-1} + b_q L^{-2}, \\ f(\alpha_q(L)) &= f(\alpha_q) + c_q L^{-1} + e_q L^{-2}, \end{aligned} \quad (20)$$

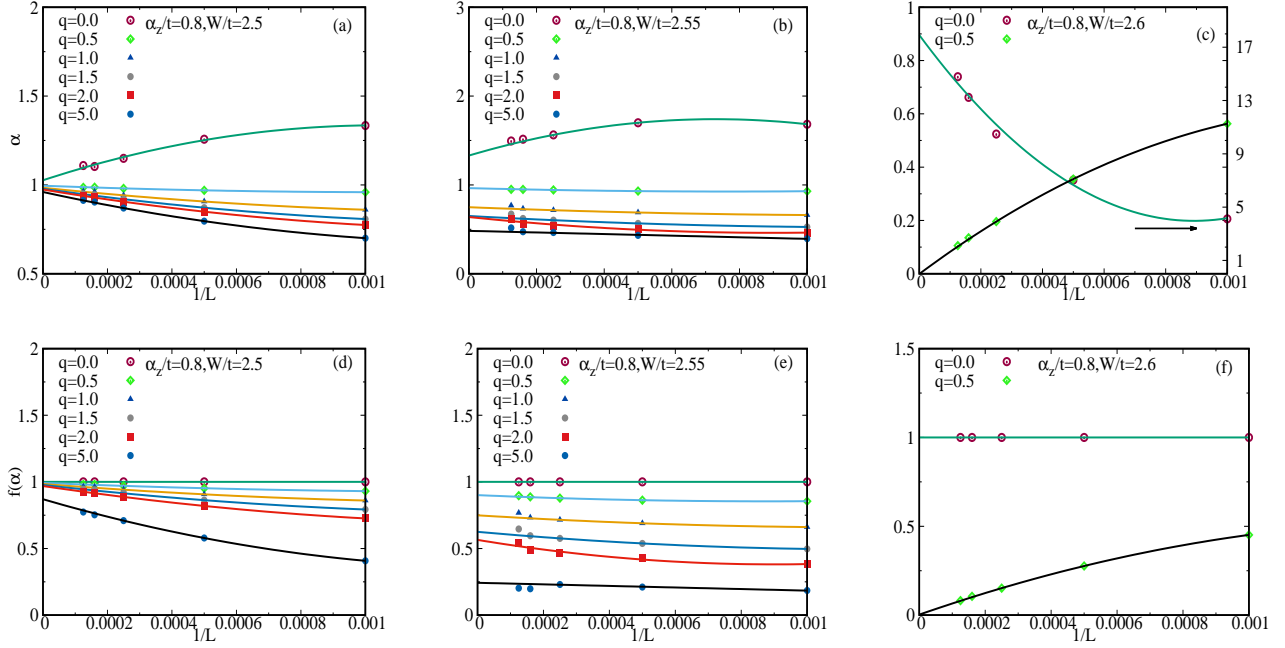


Figure 9. Top row: finite size scaling of $\alpha(q)$ with $1/L$ and bottom row: finite size scaling of $f(\alpha(q))$ with $1/L$ for some limiting values of the moment q . The scaling functions are given in Eq.20. The complex hopping amplitude $\alpha_y/t = 0$. From left to right, $W/t = 2.5, 2.55$, and 2.6 . All of these results are presented for open boundary condition.

where $\alpha_q, f(\alpha_q), a_q, b_q, c_q$, and e_q are adjustable parameters. In Fig. 9 we present results of these scaling of $\alpha_q(L)$ and $f(\alpha_q(L))$ for three different region, at the critical point and below and above it. Before discussing the scaling results, we first discuss the $f(\alpha(q))$ vs $\alpha(q)$ spectrum, presented in Fig. 8. In Fig. 8(a)-(c) we present the results for PBC, while the results with OBC are presented in Fig. 8(d)-(f). All these results are for $\alpha_z/t = 0.8$. As mentioned in earlier, one of the main purpose of presenting the results with two different boundary conditions is to demonstrate that it does not affect our fundamental conclusion about the nature of the states. Furthermore, these results indicate that one can use OBC to calculate the multifractal spectrum quite accurately using reasonably large system sizes, at least in 1D.

In Fig 8(a) and (d), $\alpha_z/t = 0.8$ and $W/t = 2.5$. From the results of localization tensor, the quasi-particle states are expected to be extended and ergodic. It is clear from the results of multifractal spectrum that, in the thermodynamic limit we have $f(\alpha(q = 0)) \rightarrow 1$, while $\alpha(q) \rightarrow 1$. These two values are not exactly 1 as one would expect for ideal extended ergodic states, but they are very close to the ideal value. Using Eq. 15 and Eq. 16 we have computed $D(2)$. As expected for metallic states, our estimated value of $D(2)$ is 0.98 (0.99) for periodic (open) boundary conditions respectively. As we increase W/t to 2.55 (Fig. 8 (b) and (e)), we can see the dramatic change in the multifractal spectrum. In the thermodynamic limit, $f(\alpha_q) \rightarrow 0$ for $\alpha(q) < 1$, while $f_{max} = f(\alpha(q = 0)) = 1$ for $\alpha(q = 0) > 1$. It clearly in-

dicates that all the states are extended, yet *non-ergodic*. This observation is also supported by our estimation of $D(2)$. At the critical point $D(2) = 0.89$ for PBC, while $D(2) = 0.93$ for OBC according to our estimate.

It is interesting to have a closer look at the behaviour of $f(\alpha_q(L))$ vs. $\alpha_q(L)$ spectrum with system size L . For different system sizes the spectrum cross each other at some point. How these spectrum move with increasing system size on either side of the crossing indicates the nature of the eigenstates. For EE and NE states, the spectrum move towards $\alpha = 1$ with increasing system size. This evolution of the multifractal spectrum with system size gets *reversed* quite dramatically as we increase the disorder strength just a little to the value $W/t = 2.6$. In this case, with increasing system size the spectrum moves towards $\alpha = 0$ on the the left of the crossing point, while on the right of the crossing point it moves further away from $\alpha = 1$. The results are presented in Fig. 8(c) and (f). It is evident that in the thermodynamic limit, $f(\alpha_q) \rightarrow 0$ for $\alpha_q \simeq 0.0$, while $f_{max} = f(\alpha(q = 0)) = 1$ for $\alpha(q = 0) \gg 1$, indicating that all the states are localized. From the numerical data, we find that $D(2) = 0.02(0.01)$ for PBC (OBC), as expected. These results are also consistent with our estimation of the critical point from the localization tensor calculations, as well as with the IPR and vNE results.

In Fig. 9, we have presented the scaling data for for $\alpha_y/t = 0, \alpha_z/t = 0.8$ and few limiting values of q . Here results are presented for OBC only. For PBC the results are nearly identical. To demonstrate the dramatic

change in the multifractal spectrum we have chosen the self dual point $W_c/t = 2.55$ and two different potential strengths just below and above it. In Fig. 9(a)-(c), $\alpha_q(L)$ has been plotted with $1/L$, while Fig. 9(d)-(f) are for $f(\alpha_q(L))$. From Fig. 9(a) it is clear that just below the critical point $\alpha_q(L) \rightarrow 1$ with increasing system size for all q . Same pattern can be observed for $f(\alpha_q(L))$ as well, although for higher q the convergence is not perfect. The convergence of $f(\alpha_q(L))$ to 1 becomes perfect as disorder strength is lowered slightly from $W/t = 2.5$. From Fig. 9(b) we can see that at the critical point $\alpha_q(L)$ and $f(\alpha_q(L))$ do not converge to a single value for different q in the thermodynamic limit. $\alpha_{q=0}(L)$ converges to a value greater than 1, while it converges to a single value much less than 1 as q increases beyond 2.0. At the same time, $\lim_{L \rightarrow \infty} f(\alpha_q(L)) \rightarrow 0$ as q is increased. This indicates that the eigenstates are extended but non-ergodic. Quite dramatically, as W/t is increased just by a small amount to 2.6, $\lim_{L \rightarrow \infty} \alpha_{q=0}(L)$ converges to a value much larger than 1, while in the thermodynamic limit $\alpha_{q \neq 0}(L)$ and $f(\alpha_q(L))$ converge rapidly to the origin at the same time with higher moment q . This indicates that the states are localized across the entire spectrum.

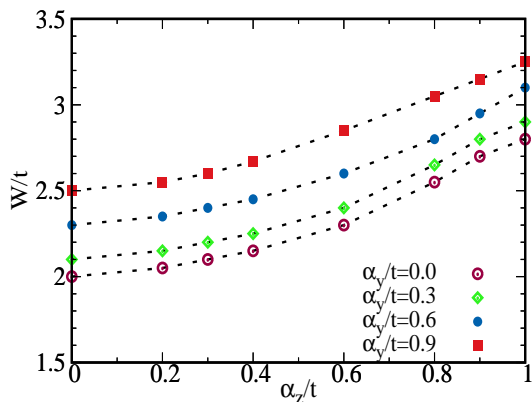


Figure 10. Phase diagram in the parameter space spanned by the strength of quasi-periodic potential W/t and the spin-flip hopping amplitude α_z/t . α_y/t represents the spin conserving complex hopping amplitude induced by RSO coupling. The dotted lines indicate the phase boundary.

VII. PHASE DIAGRAM

Finally, we present the phase diagram in the parameter space spanned by W/t and α_z/t . The phase boundaries has been obtained for increasing strength of the complex hopping of the RSO Hamiltonian. Each of these phase boundaries are indicated schematically by dotted line in Fig. 10. The phase is metallic below it, while it is an insulating phase above the boundary. On each of these boundaries, all the states are extended and non-ergodic.

VIII. CONCLUSIONS

In conclusion, we have studied the effect of RSO coupling on the critical behaviour of one dimensional quasi-periodic lattice, described by AAH Hamiltonian. We have found that RSO coupling does not affect the self-dual nature of AAH model, however the self-dual point moves towards higher strength of the quasi-periodic potential. Moreover, individual influences of the two different kinds of hopping induced by Rasha spin-orbit coupling, that is the spin conserving complex hopping and spin-flip real hopping, are identical in nature. We have found no evidence of coexistence of extended and localized states in the entire parameter space. Furthermore, the phases are insensitive towards the existence of any sub-gap states that might exist in the energy spectrum depending on the lattice size and boundary conditions. In the process of studying the MIT in this system, we have also demonstrated that can be also used to study the transition from delocalized to localized phase in system where the spin states mix and eigenstates are quasi-particles rather pure spin states. For a rigorous analysis of the eigenstates, we have performed the multifractal analysis, and it has been demonstrated that the algorithm works equally well for PBC as well OBC. This effectively removes the constraint on the system sizes that can be used to obtain the results in the thermodynamic limit for quasi-periodic systems.

IX. ACKNOWLEDGEMENT

This work is supported by SERB (DST), India (File No. EMR/2015/001227, Diary No. SERB/F/6197/2016-17). S.D would like to thank Aditi Chakrabarty for helpful feedback on the manuscript.

[1] P. W. Anderson, Phys. Rev. **109**, 1492 (1958).
 [2] E. Abrahams, P. W. Anderson, D. C. Licciardello, and T. V. Ramakrishnan, Phys. Rev. Lett. **42**, 673 (1979).
 [3] X. Deng, S. Ray, S. Sinha, G. V. Shlyapnikov, and L. Santos, Phys. Rev. Lett. **123**, 025301 (2019).

[4] P. G. Harper, Proc. Phys. Soc. London Sect. A **68**, 874 (1955).
 [5] M. Ya. Azbel, Sov. Phys. JETP **17**, 665 (1963); **19**, 634 (1964); Phys. Rev. Lett. **43**, 1954 (1979).
 [6] S. Aubry and G. André, Ann. Israel Phys. Soc. **3**, 133 (1980).

- [7] G. Roati, C. D'Errico, L. Fallani, M. Fattori, C. Fort, M. Zaccanti, G. Modugno, M. Modugno, and M. Inguscio, *Nature (London)* **453**, 895 (2008).
- [8] Y. Lahini, R. Pugatch, F. Pozzi, M. Sorel, R. Morandotti, N. Davidson, and Y. Silberberg, *Phys. Rev. Lett.* **103**, 013901 (2009).
- [9] Y. E. Kraus et al., *Phys. Rev. Lett.* **109**, 106402 (2012).
- [10] K. A. Madsen et al., *Phys. Rev. B* **88**, 125118 (2013).
- [11] Goblot, V., Štrkalj, A., Pernet, N. et al., *Nat. Phys.* **16**, 832 (2020).
- [12] S. Hikami, A. I. Larkin and Y. Nagaoka, *Progr. Theor. Phys.* **63**, 707 (1981).
- [13] S. N. Evangelou and T. Ziman, *J. Phys. C* **20**, L235 (1987).
- [14] S. N. Evangelou, *Phys. Rev. Lett.* **75**, 2550 (1995).
- [15] T. Ando, *Phys. Rev. B* **40**, 5325 (1989).
- [16] R. Merkt, M. Janssen, and B. Huckestein, *Phys. Rev. B* **58**, 4394(1998).
- [17] K. Minakuchi, *Phys. Rev. B* **58**, 9627 (1998).
- [18] K. Yakubo and M. Ono, *Phys. Rev. B* **58**, 9767 (1998).
- [19] Y. Asada, K. Slevin, and T. Ohtsuki, *Phys. Rev. Lett.* **89**, 256601 (2002).
- [20] Y. Su and X. R. Wang, *Phys. Rev. B* **98**, 224204 (2018).
- [21] E. I. Rashba, *Fiz. Tverd. Tela (Leningrad)* **2**, 1224 (1960) [*Sov. Phys. Solid State* **2**, 1109 (1960)].
- [22] I. Zutic, J. Fabian, and S. Das Sarma, *Rev. Mod. Phys.* **76**, 323 (2004).
- [23] R. Resta, *Phys. Rev. Lett.* **80**, 1800 (1998).
- [24] R. Resta and S. Sorella, *Phys. Rev. Lett.* **82**, 370 (1999).
- [25] W. Kohn, *Phys. Rev.* **133**, A171 (1963).
- [26] M. Kohmoto and D. Tobe, *Phys. Rev. B* **77**, 134204 (2008).
- [27] J. E. Birkholz and V. Meden, *Phys. Rev. B* **79**, 085420 (2009).
- [28] T. Ando and H. Tamura *Phys. Rev. B* **46**, 2332 (1992).
- [29] F. Mireles and G. Kirczenow, *Phys. Rev. B* **64**, 024426 (2001).
- [30] Ye Cao, Gao Xianlong, Xia-Ji Liu, and Hui Hu, *Phys. Rev. A* **93**, 043621 (2016).
- [31] V. K. Varma and S. Pilati, *Phys. Rev. B* **92**, 134207 (2015).
- [32] R. Resta, *J. Phys.: Condens. Matter* **14**, R625 (2002).
- [33] R. Resta, *Eur. Phys. J. B* **79**, 121 (2011).
- [34] R. Resta, *J. Chem. Phys.* **124**, 104104 (2006).
- [35] G. L. Bendazzoli, S. Evangelisti, A. Monari and R. Resta, *The J. Chem. Phys.* **133**, 064703 (2010).
- [36] S. N. Evangelou and J.-L. Pichard, *Phys. Rev. Lett.* **84**, 1643 (2000).
- [37] Y. Takada, K. Ino, and M. Yamanaka, *Phys. Rev. E* **70**, 066203 (2004).
- [38] K. Machida and M. Fujita, *Phys. Rev. B* **34**, 7367 (1986).
- [39] N. Roy and A. Sharma, *Phys. Rev. B* **100**, 195143 (2019).
- [40] F. Evers and A. D. Mirlin, *Phys. Rev. Lett.* **84**, 3690 (2000).
- [41] A. De Luca, B. L. Altshuler, V. E. Kravtsov, and A. Scardicchio *Phys. Rev. Lett.* **113**, 046806 (2014).
- [42] M. Janssen, *International Journal of Modern Physics B* **8**, 943 (1994).
- [43] E. Cuevas, *Phys. Rev. B* **68**, 024206 (2003).